Kathmandu University
Journal of Science, Engineering and Technology

Numerical analysis of draft tube vortices of Francis turbine with experimental validation

S. Basnet*[a], P. L. Bijukche[a], P. Shrestha[a], S. Chitrakar[a], and R. P. Adhikari[b]

[a]Department of Mechanical Engineering, Kathmandu University Dhulikhel, Nepal.
[b]Department of Physics, Kathmandu University, Dhulikhel, Nepal

Abstract

Although hydraulic turbines are designed for the Best Efficiency Point (BEP), turbines are mostly operated at off-designed conditions due to variation in flow and load. The turbine's efficiency decreases during the operation away from BEP. Draft tube vortices, generated while operating away from BEP are one of the causes for the decrease in efficiency, enhancing vibration problems, as well as the deterioration of the turbine in some cases. The objective of present study is to model and analyze the vortex rope formation using open source CFD codes. This paper presents numerical analysis of vortex formation in a high head Francis turbine at different operating conditions. Analysis is performed by using OpenFOAM solvers. The κ-ω SST turbulence model is employed in the Reynolds averaged Navier-Stokes's equations in this study. The computing domain includes the runner and draft tube cone, which is discretized with full three-dimensional mesh system of unstructured tetrahedral shapes. The finite volume method is used to solve the governing equations of mixture model. The tendency of vortex formation in the draft tube cone agrees well with the experimental results with an average deviation of 5.43% in the axial velocity downstream of runner. The nature of vortex is analyzed at different load conditions from 70% of BEP to 117% of BEP.

Keywords: Draft tube; Vortex rope; OpenFOAM; BEP

1. Introduction

Hydraulic turbines are generally designed to operate at Best efficiency point, where they provide maximum output. However, the fluctuating energy market has impacted in operation of hydro turbines at Best Efficiency Point. Hydro power, being able to accommodate in different operation range faster than other energy sources, is relayed for maintaining energy demand-supply chain. This leads to operation of turbines at off-designed condition. While operating turbines at off-designed condition, various effects are seen that causes drop in turbine efficiency and also deterioration of turbine unit. The study of turbine's efficiency at different loading conditions cannot be overlooked while designing the turbine.

Francis turbine, designed by James B. Francis, is one of the most popular reaction type turbines in operation [1]. The turbine efficiency is found to decrease during the operation away from best efficiency point (BEP). At part load (PL) condition, the flow field in Francis turbines become unstable in the draft tube leading to the formation of the Rotating Vortex Rope (RVR) [2]. Rheingans realized some power fluctuation due unstable flow field, especially the unsteady vortices in entrance of draft tube. Rheingas named this phenomenon the Rotating vortex rope [3]. Benjamin investigated the characteristics of swirling flow and predicted the vortex break down [4]. Cassidy and Falvery introduced the term swirl intensity as ratio of angular momentum to axial momentum [5]. The swirling flow field was visualized in draft tube by Nishi et.al [6] and stated development of stalled region in entrance of draft tube due to decrease in flow rate. Stall region grows, merges, rotates and moves down when turbine operates in part load. RVR is actual consequences of high shear on the interference between the recirculation of central region and the main flow and causes a low frequency and high amplitude pressure fluctuation. Escudier investigated the existence of RVR rotation which affect rotation and make the flow field unsteady [7]. Trivedi et al [8] investigated the pressure field unsteadiness in the runner, vaneless space, and draft tube due to the guide vane's angular movement.

Theoretically, at the best efficiency point, the flow leaving the runner and ingested by the draft tube is almost purely axial as in Fig. 1(b) (where V_t= 0 and V=V_a). So, a certain level of residual swirl is taken at runner outlet to prevent flow separation from the draft tube wall and to minimize hydraulic losses associated with kinetic energy-to-static pressure conversion in the draft tube. This swirling flow at the draft tube inlet is tuned for optimal performance at the best efficiency operating point. However, the swirl ingested by the draft tube departs significantly from the best configuration as the turbine discharge varies, and Francis turbines, operating at off-design conditions often have a high residual swirl at the draft tube inlet [1].

In Fig. 1, U is the runner velocity, W is the relative velocity, and V is the absolute velocity leaving the runner and ingested by the draft tube, with V_a and V_t being axial and circumferential (swirl) components. Depending on the operating conditions, two forms of the flow instability can be observed. At part load conditions, for which the flow rate is lower than the one at the BEP, the flow has a positive absolute circumferential velocity in the same sense as the runner revolution (where V_t and U are in the same direction in velocity triangle of Fig. 1(a)). In this case a helical processing vortex called the "vortex rope" develops in the draft tube. At full load conditions corresponding to a higher flow rate than that of the BEP, the absolute circumferential velocity is negative inducing a swirling flow rotating in the opposite direction of the runner (as in velocity triangle of Fig. 1 (c) where V_t and U are in opposite di-

*Corresponding author. Email: basnyaatsaroj777@gmail.com

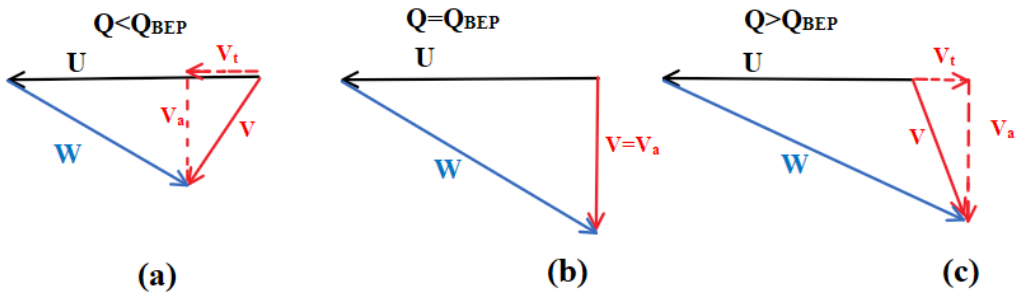

Figure 1: Velocity triangles at runner exit (a) part load (b) best efficiency point and (c) full load.

Table 1: Mesh statistics.

Mesh	M1	M2	M3	M4	M5
Elements (in millions)	1.453	2.217	3.753	5.119	10.899
Nodes(in millions)	0.412	0.612	1.000	1.339	2.759

rection). In this case, the vortex rope takes a nearly axisymmetric shape, sometimes called the "torch". The physical mechanism of vortex rope formation is termed as "vortex breakdown" [9].

In this paper, an attempt has been made to visualize the vortex formation at different operating conditions. The use of an openFOAM based on Finite Volume Method has been focused for the study. The geometry is based on previous research works; whose experimental data is available for validation.

2. Materials and method

2.1. Geometry

The high head Francis turbine model studied in Francis-99 workshop was taken into study in this work. The turbine model was provided by NTNU – Norwegian University of Science and Technology under the Francis-99 workshop series [10]. Francis-99 is a series of three workshops, which provides an open access of the complete design and data of a model Francis turbine. The Francis-99 turbine is a reduced scale (1:5.1) model of a prototype operating at the Tokke power plant, Norway. The turbine geometry includes 14 stay vanes integrated inside the spiral casing, 28 guide vanes, a runner with 15 blades and 15 splitters, and an elbow-type draft tube [11].

Fig. 2 (a) is the reference coordinate system. The measurement of velocity and pressure were performed at a red colored horizontal line, Line1, 64 mm below runner base in draft tube cone, as shown in Fig. 2 (b). The end points having (X, Y, Z) coordinates of the line1 were taken as. (-0.1789,0, -0.2434) and (0.1789,0, -0.2343). Necessary parameters were calculated over 400 uniformly distributed points over the Line1.

2.2. Grid generation

For the numerical simulation, only runner and draft tube cone was taken into account (Fig. 3). The runner geometry had 15 runner blades and 15 splitters. The geometry was combined as one domain in order to apply SRF (Single Reference Frame) properties. ANSYS Meshing tool was used for creating unstructured tetrahedral mesh of the geometry. Statistics of the mesh used are shown in Table 1.

Table 2: Patches and boundary condition applied.

Patches	p	$\mathbf{U}_{\text{rel}}$
inletr	zeroGradient	cylindricalInletVelocityuniform (0 0 0)
outletc	fixedValueuniform 0	pressureInletOutletVelocity uniform (0 0 0)
blades	zeroGradient	noSlip
wallr	zeroGradient	noSlip
wallc	zeroGradient	noSlip

2.3. Mesh independence study

Mesh independence study was based on maintaining the size of the mesh element varying at a growth rate of 1.3 to 1.5, while keeping the same mesh distribution in the fluid domain. The variation in the mesh size was carried out according to the guidelines provided by Celik et. al [12]. Because of unstructured type of the grids used in the fluid domain, the total element between successive mesh is different. Grid independence verification of the pressure and axial velocity at BEP was performed. These results are shown in Fig. 4. The pressure and axial velocity are obtained at Line1 by varying only number of elements at BEP condition. In this study, grid size having 2.217M element was chosen for the further numerical study. Fig. 4 (a) and (b) shows the dynamic pressure ($\frac{p}{\rho}$) plotted against diameter (x) and axial velocity plotted against normalized diameter ($\frac{r}{r_0}$) respectively.

2.4. Boundary condition

The simulation was done using SRFSimpleFoam solver. Stationary components (guide vane, spiral casing domain and draft tube) were not taken into account. Inlet was provided at the rim of runner. The outlet was taken at the surface connecting the cone and the draft tube. Other components were taken as walls with no-slip condition. The patch names, inletr, outlet, blades, wallr and wallc were given for inlet, outlet, blades, runner wall and cone wall respectively. The names of the boundary conditions are illustrated in Fig. 5, with their values in Table 2 where p is the pressure and $U_{\text{rel}}$is relative velocity.

2.5. Loading condition identification

Loading conditions were selected as per the mass flow rate at inlet given by the experiments of Francis-99 workshop [10]. Part load and full load were taken at 71% of BEP and 117% of BEP respectively. Mass flow of 200.5 kg/s was taken as 100% of BEP in experiment and corresponding radial velocity -1.7 m/s was obtained through graph. The rpm in U_{rel} corresponded to the tangential velocity and thus was taken as 0 as flow is parallel to the surface of the blade. For all the other conditions, a graph shown in Fig. 6 was referred to find

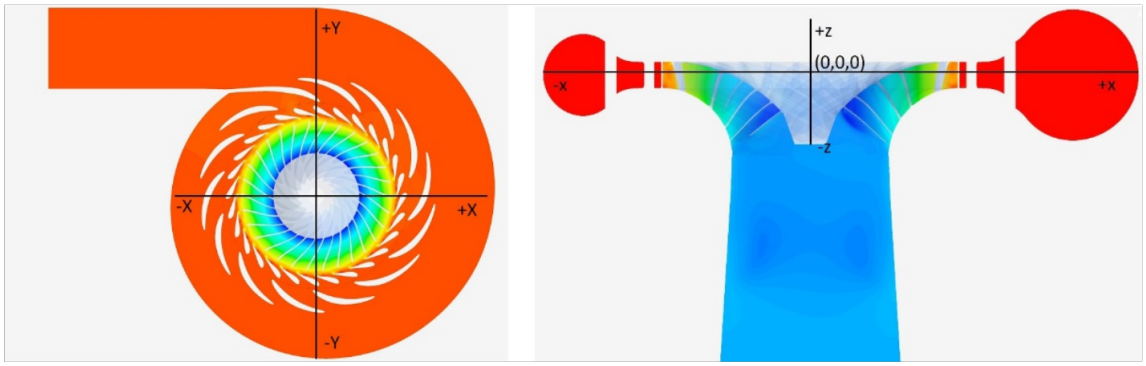

(a)

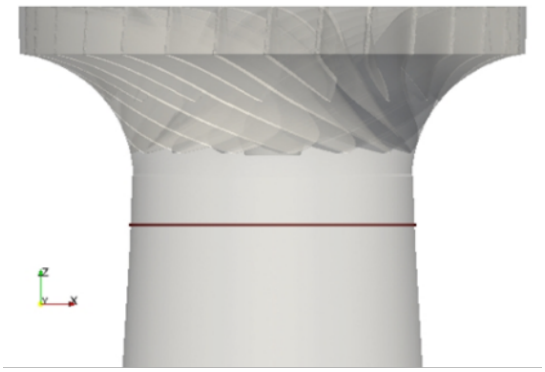

(b)

Figure 2: (a) Reference coordinate system and (b) Line 1 in Draft tube cone for studying the velocity/pressure distribution (Adapted from [10]).

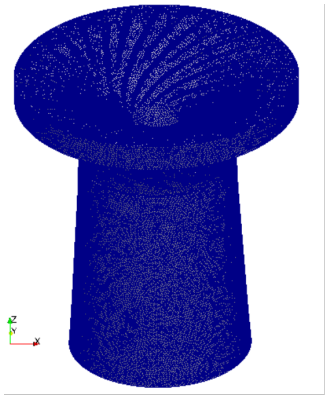

a)

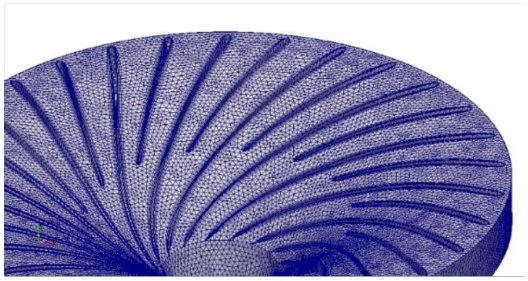

b)

Figure 3: (a) Mesh used for the simulation (M2) and (b) inflation around the blade region

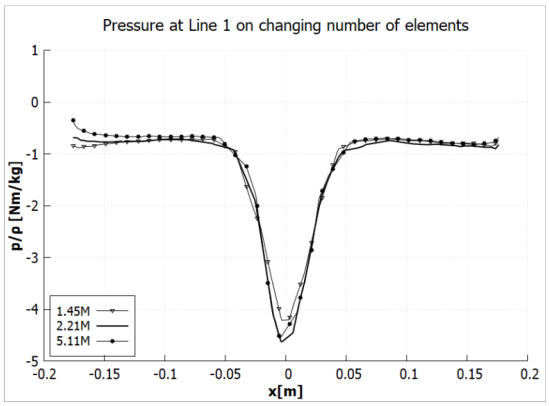

(a)

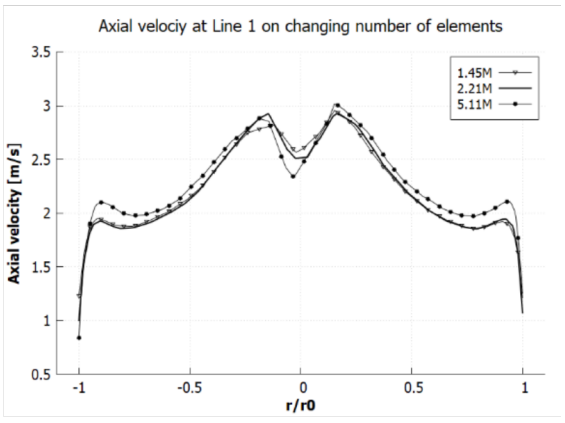

(b)

Figure 4: Study of varying element size on (a) dynamic pressure (b) axial velocity.

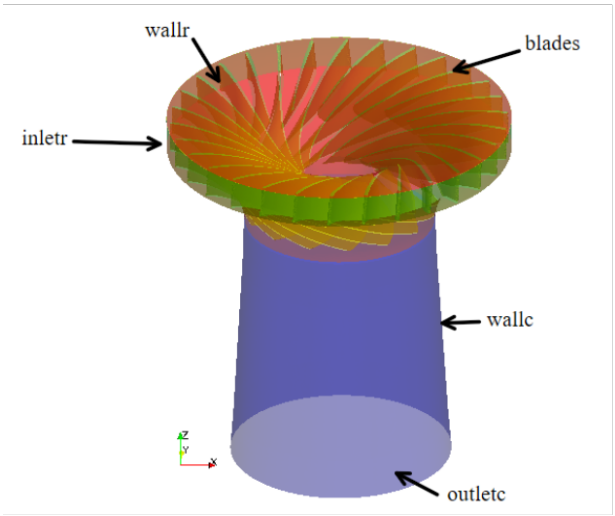

Figure 5: Patches used to define the components.

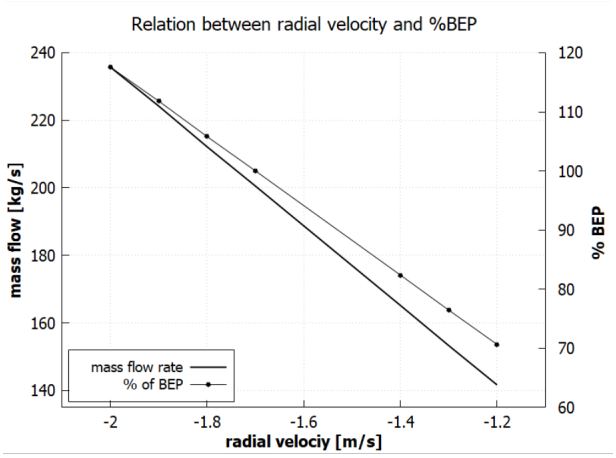

Figure 6: Relation between radial velocity and mass flow at inlet.

the determine the value of radial velocity corresponding to the required flow rate and the condition relative to BEP at 100%.

3. Results and discussion

3.1. Validation with experimental result

Comparison of result with experimental values was performed from the available resources. The experimental data were recreated from the paper of M. Raddahian et.al [11]. The axial velocity was plotted over normalized diameter at BEP condition as in Fig. 7. The values for axial velocity were obtained at BEP condition over the Line1. Square dot points are the recreated experimental values and continuous line is the result from numerical study.

The numerically obtained result of axial velocity follows the trend of experimental result with average deviation of 5.483% from experimental value. The axial velocity tends to increase toward the central region with a sudden drop at the center. This effect is the result of development of vortex at the central region. The vortex formed at BEP has comparatively less intensity compared to full load conditions.

3.2. Study on various Turbulence model

Turbulence model create a significant difference in result while doing numerical analysis. Fig. 8 shows comparison between tur-

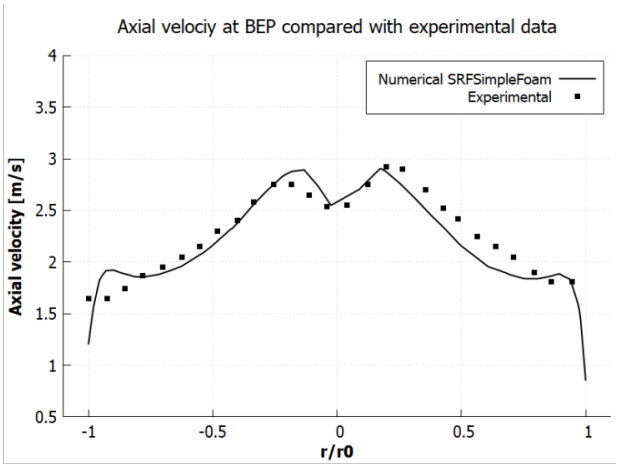

Figure 7: Axial velocity at BEP compared with experimental data.

Table 3: Comparison of setting in two solvers.

Parameter	Solver1	Sovler2
Calculation type	Steady state	Steady state
Turbulence model	κ-ω SST	κ-ω SST
BC input/output	Cylindrical inlet velocity/pressure	Cylindrical inlet velocity/pressure
Solution control	Selected time step	Default under relaxation factors

bulence models implied in the study. κ-ω SST, realizable $\kappa\epsilon$ and κ-Epsilon were three turbulence model taken into account. The pressure at line 1 shows κ-Epsilon and κ-ω SST could capture the pressure drop effectively. However, the axial velocity was better plotted by κ-ω SST.

Result of κ-ω SST also better satisfies with the experimental data. Additionally, other researchers also found κ-ω SST being able to capture the physical effects better than other turbulence models. κ-ω SST was used on all other simulations in this study.

3.3. Study of different solvers

A comparison between two different solvers was done. Solver1 uses SRFSimpleFoam of OpenFOAM and Solver2 uses ANSYS-CFX. Simulations were done keeping all the physical conditions constant. The varying condition can be noted as the auto timestep suppression of solver2. The solution in Solver1 was run until solution convergence is satisfied. The comparison of the settings in solver can be found in Table 3.

Fig. 9 shows the results at BEP condition on both solvers. The pressure drops over Line1 is better captured by solver1 while it is suppressed in case of solver2. The reason for the variation can be due to advance residual control system in solver2, whose code is not fully available for public visualization.

3.4. Study by varying loading condition

The formation of pressure drop zones at different load and speed conditions was studied. The effect of varying the speed of runner on the characteristics of draft tube was studied for the case of inlet velocities corresponding to BEP.

3.4.1. Varying speed at BEP condition

Change in the distribution of pressure and velocity downstream of the runner on varying the rotational speed of turbine from 300

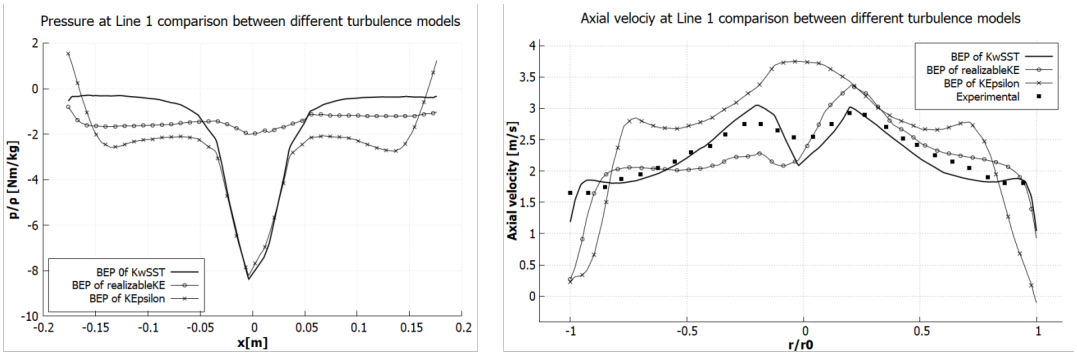

(a) (b)

Figure 8: Study on different turbulence models (a) dynamic pressure line (b) axial velocity.

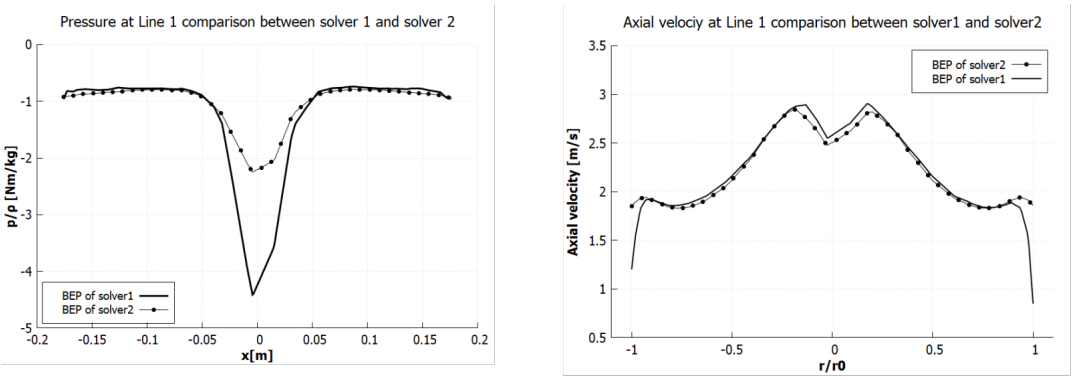

(a) (b)

Figure 9: Study on different solvers (a) dynamic pressure (b) axial velocity.

rpm to 350 rpm was observed. The base case was taken as per the experimental case, i.e., 330 rpm. Fig. 10 shows the pressure and velocity trend at Line1 respectively. The pressure drop trend is similar while varying the rpm. Strong pressure drop is seen at the center of the cone at base point which is due to the formation of vortex. At constant mass flow rate inlet, the vortex formation region (pressure drop zone) is found to be stronger on decreasing the rotational speed.

The resultant of U_{rel} calculated at Line1 shows an abrupt drop in velocity at center region. The drop rate is higher for lower speed and lower for higher speed. The velocity increase near the wall region can be the effect of SRF property implied in the study. In the actual scenario, cone of the draft tube remains as a stationary region, because of which, the flow field around the wall region does not have high velocities. In the case of SRF model, the cone is made to rotate with the same speed as that of runner. As a result, the flow field near the wall of cone rotates together, increasing the velocity in these regions.

3.4.2. Varying mass flow rate at inlet

BEP being 100% of the designed flow rate, other conditions are defined as per Fig. 6. The extreme part load condition was taken as 71% of BEP and full load condition was 117% of BEP.

Simulations at different part load conditions was done by varying the mass flow. 70% of BEP, 76% of BEP and 82 % of BEP were provided at inlet. Fig. 11 (a) shows the pressure plots of different load at Line1 plotted along with BEP. The intensity of pressure drop was found to be in reverse order. This can be due to rotation of vortex along with the domain as the cone is also set to rotation in SRF model. In real practical case, the cone is stationary, which was not implied in the study due to the nature of this solver.

Variation of radial velocity in full load condition was observed. 105% BEP, 111% BEP and 117% BEP are observed. Fig. 11 (b) shows the pressure at Line1 at different full load condition plotted along with BEP condition. The pressure drop at the center region grows stronger on increasing the mass flow. This trend signifies the development of strong vortex torch at full load condition.

3.5. Vortex visualization at different loading condition

Fig. 12 shows the vortex formation at BEP, part load (70% BEP), and full load (117% BEP) conditions respectively. Fig. 12 (a) shows a faint vortex is developing straight downwards from the runner to the cone. The vortex even vanishes after a short length.

At part load condition (71% BEP), the low-pressure zone was found to be rotating along the direction of rotation of domain. In this case, a helical processing vortex called the “vortex rope” develops in the draft tube, which can be visualized in Fig. 12 (b). At part load conditions, for which the flow rate is lower than the one at BEP, the flow has a positive absolute circumferential velocity, same as the runner revolution. Thus, the formation of helical rope occurs.

At full load (117% BEP) condition, the vortex developed stronger than that at BEP condition. The formation of vortex torch can be seen in Fig. 12 (c). At full load conditions corresponding to a higher flow rate than that of the BEP, the absolute circumferential velocity is negative inducing a swirling flow rotating in the opposite direction of the runner. In this case, the vortex rope takes a nearly axisymmetric shape, called the “torch”.

4. Conclusion

This research work focused on the use of opensource software, OpenFOAM to study and analyze the formation of vortex using SRF-

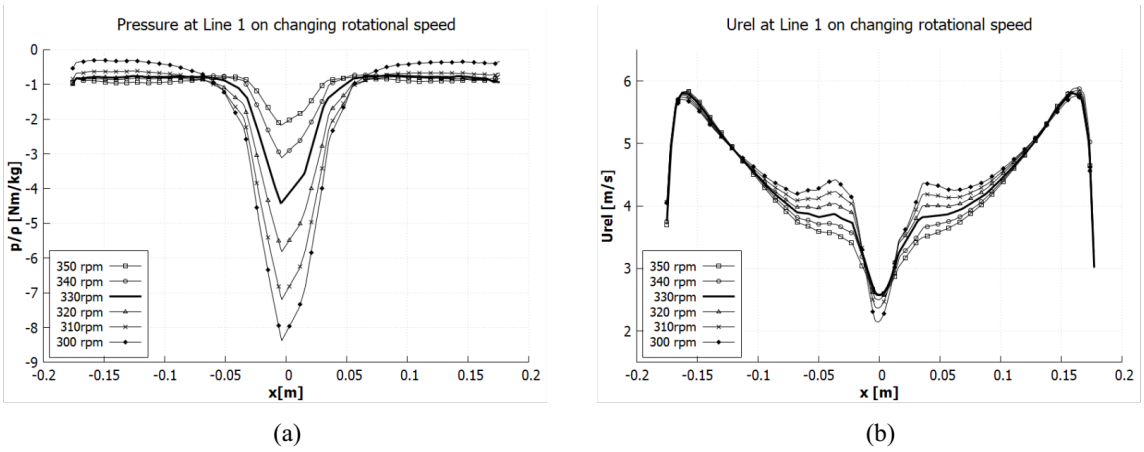

Figure 10: Study on varying rpm at BEP condition (a) dynamic pressure (b) resultant of relative velocity.

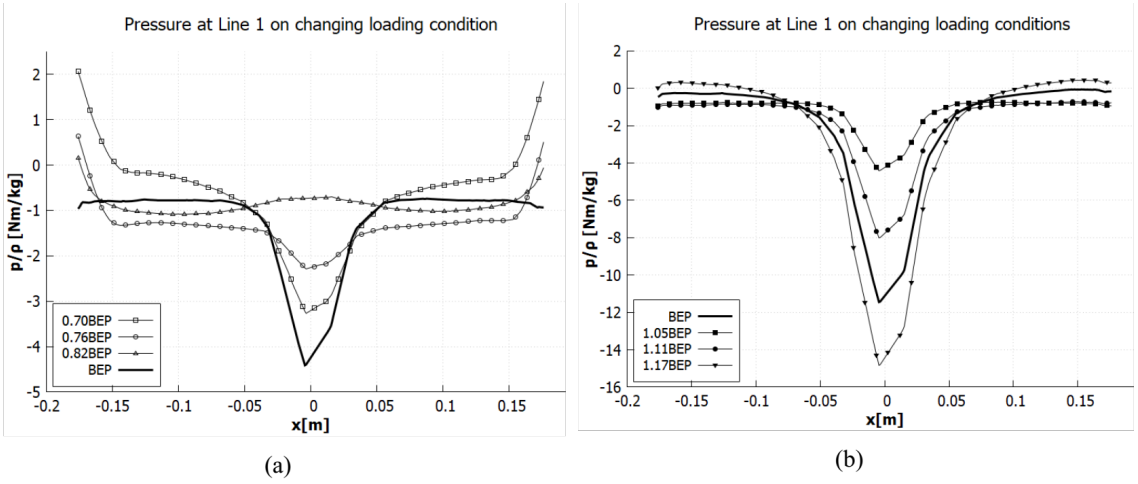

Figure 11: Studying on varying mass flow rate at inlet Dynamic pressure plot (a) on various low load conditions (b) on various high load conditions.

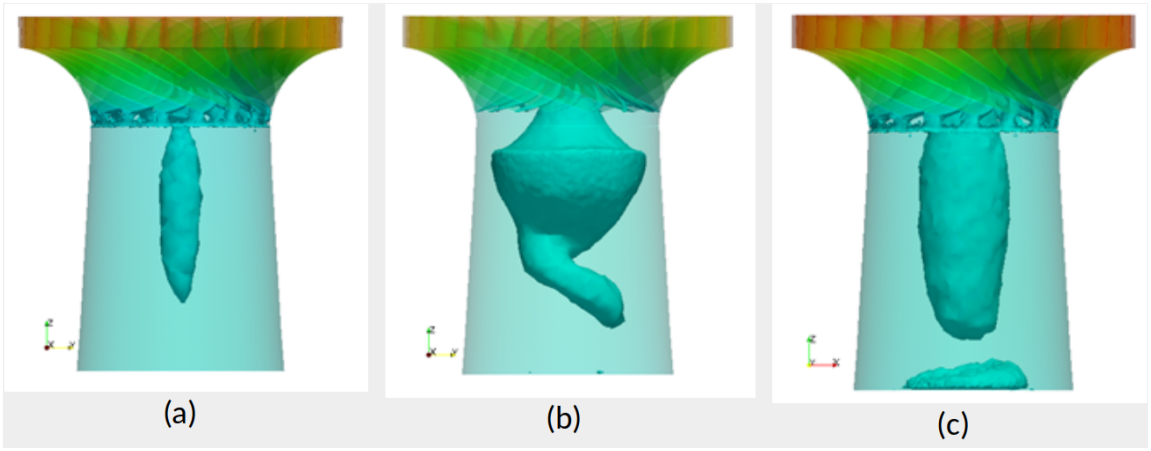

Figure 12: Visualization of vortex (a) at BEP condition (b) at part load (c) at full load.

SimpleFoam solver of OpenFOAM. The goal was to visualize the type and intensity of vortex formed at different loading and rotational speed conditions. Steady state study was performed with satisfying results and its validation with experimental data. The performance of OpenFOAM was found to be equivalent to that of commercial software. The physics behind the formation of vortices in draft tube was studied and simulations were performed to visualize the vortices numerically. The result from numerical study showed good relation with experimental values for axial velocity at BEP condition with average deviation of 5.483%. Three-part load conditions, with mass flow rate of 0.7BEP, 0.76BEP and 0.82BEP, were studied. Helical processing vortex was obtained while simulating at part load condition. The vortex rope was found to be rotating in the same direction as the runner. Three full load conditions with mass flow rate of 1.05BEP, 1.11BEP and 1.17BEP, were studied. The formation of vortex was straight and faced downwards from the runner. The study was limited by the use of SRFSimpleFoam solver, in which whole domain in the draft tube cone region was set to rotation along with the runner domain.

Acknowledgment

We used the test-case provided by NTNU – Norwegian University of Science and Technology under the Francis-99 workshop series.

References

[1] Subramanya K, Hydraulic Machines, Tata McGraw-Hill Education Pvt. Limited, 2013.

[2] Foroutan H, Simulation, Analysis, And Mitigation of Vortex Rope Formation in the Draft Tube of Hydraulic Turbines, The Pennsylvania State University, 2015.

[3] Rheingas W, Power swings in hydroelectric power plants, *ASME,* 62(3) (1940) 171-184.

[4] Benjamin T, Theory of the vortex breakdown phenomenon, *Journal of Fluid Mechanics,* 14(4) (1962) 593-629.

[5] Cassidy J & Falvey H, Observation of unsteady flow arising after vortex breakdown, *Journal of Fluid Mechanics,* 41(4) 727-736, 1970.

[6] Nishi M, Flow regimes in an elbow type draft tube, *IOP Conference Series: Earth and Environment Science,* 982 (1928) 38.

[7] Escudier M, Confined vortices in flow machiery, *Annual Review of Fluid Mechaincs,* 19(1) (1987) 27-52.

[8] Iliev I, Chirag T & Dahlhaug O G, Variable-speed operation of Francis turbines: A review of the perspectives, *Elsevier,* 2019.

[9] Hall M, Vortex Breakdown, in *Annual Review of Fluid Mechanics 4*, Farnborough England, 1972, pp. 195-218.

[10] Norwegian Hydropower Centre, Test Case Experimental Study- Francis 99, 2014. [Online]. Available: https://www.ntnu.edu/nvks/f99-test-case1. [Accessed dec 2019].

[11] Maddahian R, Sotoudeh N & Cervantes M J, Formation of Rotating Vortex Rope in the Francis-99 Draft Tube, in *IOP Conference Series: Earth and Environmental Science*, 2019.

[12] Celik I, Ghia U, Roache P, Freitas C, Coleman H & Raad P, Procedure for Estimation and Reporting of Uncertainty Due to Discretization in CFD Applications, *Journal of Fluids Engineering,* 7 (2008) 130.